

Bond Rearrangement Produces Oxygen from Carbon Dioxide

Kamal Kumar , Jibak Mukherjee, Harpreet Singh and Deepankar Misra * 

Department of Nuclear and Atomic Physics, Tata Institute of Fundamental Research, Mumbai 400005, India; kamal.kumar@tifr.res.in (K.K.); jibak.mukherjee@tifr.res.in (J.M.); harpreet.singh@tifr.res.in (H.S.)

* Correspondence: dmisra@tifr.res.in

Abstract: We present a direct observation where fragmentation of the CO_2^{2+} dication, upon highly charged ion impact, leads to the formation of molecular oxygen. We assert that molecular bending and bond stretching modes of the dication represent the underlying mechanisms driving the generation of O_2^+ . We conducted ab initio quantum chemistry calculations for the electronic state of the dication and found that the 5A_1 state is responsible for the bond-rearrangement reaction. The branching ratios of this channel for multiple projectile beams of varying charge and velocity have been reported and are found to be independent of the projectile's charge and velocity.

Keywords: electron capture; bond rearrangement; potential energy curves; kinetic energy release

1. Introduction

The essential role of organisms like plants and algae in producing O_2 through photosynthesis is vital for sustaining life on Earth. Due to the dominant presence of CO_2 gas on Mars, research has been going on to produce oxygen from CO_2 , to consider Mars as a habitable planet other than Earth [1]. CO_2 is a linear triatomic molecule, and its two- and three-body fragmentation has been studied from a fundamental point-of-view by various groups in the recent past [2–5].

Initially, Chueh et al. [6] documented the generation of CO and O from CO_2 through photon absorption. However, subsequent theoretical simulations in [7,8] introduced the possibility of producing O_2 from CO_2 . A later study by Lu et al. [9] revealed the creation of O_2 through a roaming mechanism during the photo-dissociation of CO_2 molecules.

Wang et al. [10] reported the formation of molecular oxygen by dissociative electron attachment to CO_2 . They used velocity map imaging to detect C^- anions and O_2 ($X^3\Sigma_g^-$). They have reported that the roaming mechanism was responsible for O_2 production. Several investigations have also highlighted the production of O_2^+ via bond rearrangement through laser–molecule interaction [11–13], due to core hole excitation by photons [14–16], with the excitation pathways involving $\text{C } 1s \rightarrow \pi^*$ or $\text{O } 1s \rightarrow \pi^*$ transitions, the lifted degeneracy of the Renner–Teller split initially bent A_1 and linear B_1 states is responsible for the bond rearrangement [14,15]. Additionally, O_2^+ was observed as the fragmentation product of the core-level photo-excitation of CO_2 [14]. Furthermore, Larimian et al. [11] observed O_2^+ signatures during photo-double-ionization. They explained the production of O_2^+ as a two-step process involving the cation populating an electronic state with a bent geometry, followed by a second ionization leading to the new bond formation and fragmentation into C^+ and O_2^+ . Surface-collision-induced transformation of CO_2 into O_2 was also reported by Yao et al. [17]. Recently, Ganguly et al. [18] reported enhanced O_2^+ production from CO_2 clusters induced by X-ray core-electron ionization. They attributed this enhancement to intra-cluster collisions. To date, all the reported studies have centered on light-molecule interactions for molecular oxygen production. Notably, there is one study, to the best of our knowledge, by Yuan et al. [19], in which the authors reported on molecular oxygen formation due to ion–molecule interaction. They observed O_2^+ coinciding with C^+ upon a 1 keV/u Ar^{2+} beam. However, the dynamics underlying O_2^+ formation upon ion impact



Citation: Kumar, K.; Mukherjee, J.; Singh, H.; Misra, D. Bond Rearrangement Produces Oxygen from Carbon Dioxide. *Atoms* **2024**, *12*, 25. <https://doi.org/10.3390/atoms12040025>

Academic Editor: Kanti M. Aggarwal

Received: 4 March 2024

Revised: 30 March 2024

Accepted: 1 April 2024

Published: 17 April 2024



Copyright: © 2024 by the authors. Licensee MDPI, Basel, Switzerland. This article is an open access article distributed under the terms and conditions of the Creative Commons Attribution (CC BY) license (<https://creativecommons.org/licenses/by/4.0/>).

were not presented in their study. Also, the electronic state responsible for the channel was not reported. In addition, the effect of the projectile's charge and velocity on the strength of this bond rearrangement channel has also not been studied anywhere.

A study of the systematic variation of the fragmentation process by various projectile ions having different velocities and charge states in highly charged ion (HCI) molecule collisions is desirable. In HCI collisions, perturbation strength ($\eta = q/v_p$), where q is the charge state, and v_p is the velocity of the projectile ion is the governing parameter in the collision process. It also is a control parameter for the energy deposition into the system. Therefore, it is expected to influence the population of the different excited states of the molecule.

In this study, we conducted a comprehensive investigation combining experimental and theoretical approaches to understand the dynamics involved in the generation of O_2^+ upon interaction with highly charged ions with the neutral CO_2 molecules. Our study also specified the electronic state that plays a pivotal role in this process. We also studied the branching ratio between the $C^+ + O_2^+$ channel and the summation of the bond rearrangement channel with the most probable $O^+ + CO^+$ channel for projectile ions of different charges and velocities.

2. Experimental Methods

We employ coincidence detection measurement between fragmented ions and scattered projectile ions. The present experiments were performed in a cold target recoil ion momentum spectrometer (COLTRIMS) [20,21]. We used the 14.5 GHz Electron Cyclotron Resonance based Ion Accelerator (ECRIA) facility at TIFR Mumbai [22] to produce projectile beams of different velocities and charges. The target beam of CO_2 was prepared by a supersonic molecular jet setup, which consists of a nozzle of 30 μm , and two subsequent skimmers of the inner diameter of 400 μm and 1500 μm , respectively. A zone of silence was created just behind the first skimmer, and the high diverging part of the beam was cut down by the second skimmer placed at a distance of 100 mm from the first one. All the chambers were differentially pumped. Projectile and target beams were crossed with each other at the interaction region of our COLTRIMS setup [23,24] at TIFR Mumbai. After the interaction, the scattered projectile beam, which captured one or two electrons, passes through an electrostatic charge state deflector and is detected on a time- and position-sensitive MCP-DLD (micro-channel plate-delay line anode) detector in Chevron configuration, with MCP having a diameter of 80 mm. For the detection of recoil ions, we used a Wiley–McLaren type double field spectrometer with MCP-DLD. The length of the extraction region, acceleration region, and field-free drift region are 15 mm, 90 mm, and 520 mm, respectively. The electric field in the extraction and acceleration regions were set to 173.33 V/cm and 250.67 V/cm, respectively. With this configuration, singly charged ions up to 13 eV kinetic energy were recorded with 4π collection, and a KER resolution of around 250 meV was achieved for this channel of interest. Background pressure of 6.2×10^{-9} mbar was maintained in the interaction chamber. While performing the experiment with a Xe^{10+} ion beam, the interaction chamber pressure increased to 6.48×10^{-9} mbar. The projectile beam current during experiments was kept in the range of 50–250 pA. For data acquisition, the signal from the projectile MCP was used to start the data acquisition, and the last recoil ion hitting the target MCP gave the stop signal. Data were recorded in list mode files (.lmf) in an event-by-event mode for further offline analysis. From the recorded time- and position information, we calculated the momenta of each recoil ion along the three axes and calculated physical quantities of interest, such as KER and angular distribution of fragments.

In order to find the branching ratio between the two channels, an accurate estimation of the yields of a particular channel is crucial. The coincident events were selected from the coincident time-of-flight spectrum. The coincidence spectrum may also include random coincidence events. To subtract the random coincidence events, we used the conservation of momentum between ions created from the fragmentation of a single molecule.

3. Results and Discussion

The coincidence map, which is a two-dimensional plot between times-of-flight of the first and second fragment ions is shown in Figure 1. The channel of interest is shown inside a red square in Figure 1a for Xe^{10+} impact. O_2^+ can be generated from two different channels, first, after the breakup of CO_2^{2+} , which would contribute to true coincidences, and second, from the single electron capture of background oxygen which might blend with C^+ . To remove the background contamination and random coincidences, we selected the events using the conservation of momentum. After removing the background, Figure 1b displays the noise-free coincidence trace of the channel.

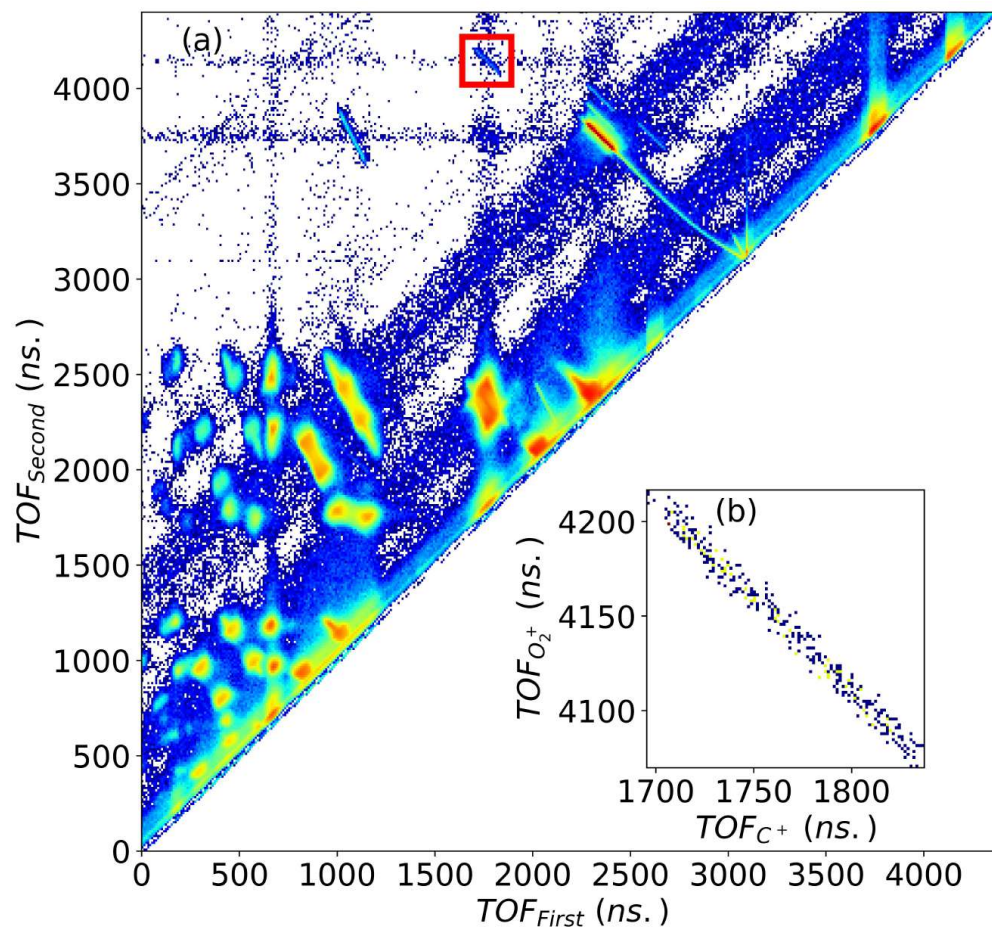


Figure 1. (a) Coincidence map of first and second recoil ions generated during the fragmentation of $\text{CO}_2^{2+} \rightarrow \text{C}^+ + \text{O}_2^+$ upon 200 keV Xe^{10+} , inside the red box is the trace corresponding to $\text{C}^+ + \text{O}_2^+$ channel, (b) $\text{C}^+ + \text{O}_2^+$ channel after background suppression by using the momentum conservation of recoiling C^+ and O_2^+ ions.

In a further analysis, we plotted the KER distribution in Figure 2a. KER is the sum of the kinetic energies of the individual fragments in a dissociation process. The spectrum starts from around 3 eV and extends up to 10 eV. There is a prominent peak around 6 eV and a broad structure from 7 eV to 10 eV, which indicates that many electronic states might contribute to this channel. We have fitted these two peaks in the KER distribution with Gaussian profiles, one at around 6 eV and the other at around 8 eV. Peak 1 is centered at $5.74 \pm 0.20 \text{ eV}$ and Peak 2 at $7.64 \pm 0.62 \text{ eV}$. However, because of low statistics for Peak 2, we would focus on the prominent peak at $5.74 \pm 0.20 \text{ eV}$ only.

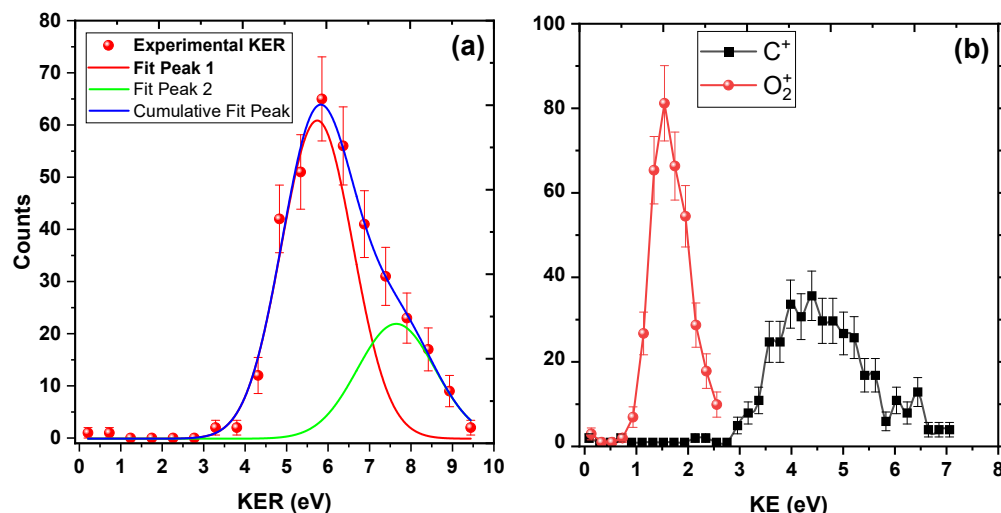


Figure 2. KER distribution upon 200 keV Xe^{10+} impact. (a) KER distribution for $\text{C}^+ + \text{O}_2^+$ channel. Two peaks around 6 eV and 8 eV are fitted with Gaussian function (see text). (b) Kinetic energy distributions of individual C^+ and O_2^+ ions. The solid lines joining the experimental data points are to guide the eye.

3.1. Dynamics

We propose that the symmetrical stretching and bending of the two C–O bonds lead to new bond formation between the two O atoms. To support this proposal, we utilize the following approach to provide insights into the bond-rearrangement dynamics: following the collision with Xe^{10+} , the CO_2^{2+} dication emerges, either in its ground state or in one of the excited electronic states in the Franck–Condon region. Subsequently, this dication undergoes stretching and bending motion, eventually leading to the formation of a new bond between two O atoms, following which the C^+ and O_2^+ fragments separate. A visual representation of this mechanism can be found in Figure 3. Since neutral carbon dioxide is a linear molecule, if this molecule breaks into O, C, and O atoms, the central C atom would carry almost negligible energy, and the two O atomic fragments would share all the deposited energy. From Figure 2b, the C^+ ion carries kinetic energy of around 4.2 eV, which experimentally proves our assertion that there lies an intermediate CO_2^{2+} ion that is bent, because of which after fragmentation the C^+ carries non-negligible kinetic energy.

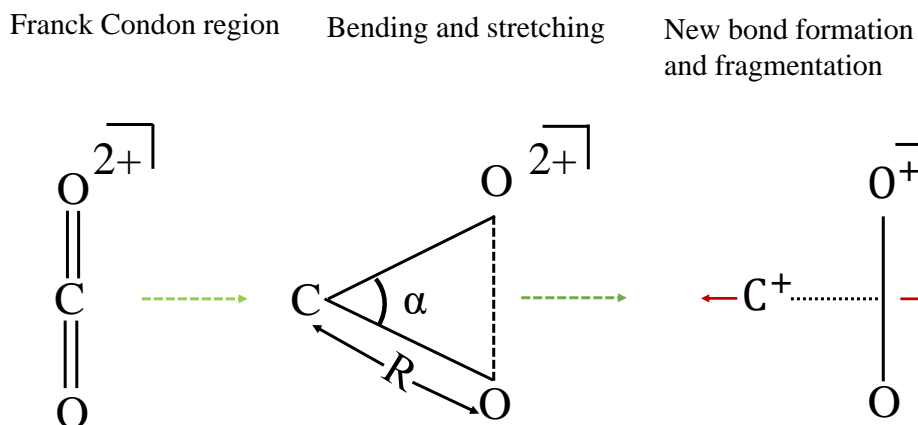


Figure 3. Scheme for bond reformation, R is the bond length of C–O bond and α is the bond angle $\angle\text{OCO}$. The intermediate triangular geometry of CO_2^{2+} favors the new bond formation.

3.2. Theoretical Calculations

Following the approach mentioned in Figure 3, we first identified the electronic state responsible for KER at around 5.74 ± 0.20 eV, using CFOUR software program [25]. We employed equation-of-motion coupled cluster singles and doubles (EOM-CCSD) method [26–29], with correlation-consistent polarized valence double zeta (cc-pVTZ) [30] basis set. We calculated single-point energies at the Franck–Condon region and at the dissociation limit, in order to match the experimental KER with the computed one. We calculated the single point energies in singlet, triplet, and quintet manifolds, of which we found out that the 5A_1 state which is the first excited state with the quintet multiplicity, corresponds to the KER value of 5.57 eV; this calculated KER lies close to the experimental one of 5.74 ± 0.20 eV. During the collision process the transition from singlet neutral ground state to the quintet excited state of CO_2^{2+} appears to violate spin conservation. We note that in the electron-capture process in the present experiments, the spin of captured electrons is not known, therefore, we can not deduce whether the bond-rearrangement process in present experiments is the spin-allowed or spin-forbidden process. The electronic configuration of the ${}^1\Sigma_g^+$ ground state of CO_2 neutral is $(1\sigma_g)^2(1\sigma_u)^2(2\sigma_g)^2(3\sigma_g)^2(2\sigma_u)^2(4\sigma_g)^2(3\sigma_u)^2(1\pi_u)^4(1\pi_g)^4$ and that of the 5A_1 state of CO_2^{2+} is $(1\sigma_g)^2(1\sigma_u)^2(2\sigma_g)^2(3\sigma_g)^2(2\sigma_u)^2(4\sigma_g)^2(3\sigma_u)^2(1\pi_u)^2(1\pi_u)^1(1\pi_g)^1(1\pi_g)^1(2\pi_u)^1$.

We tried to find out any existing transition state for the bond-formation reaction. We used second-order Moller–Plesset (MP2) theory [31] accompanied with cc-pVDZ [30] basis set to find out the minimum of the potential for 5A_1 state and searched for any existing transition state for this channel. All calculations including single point energy, optimization, and transition state search were performed under the unrestricted Hartree–Fock (UHF) method [32], and the two C–O bonds and the $\angle\text{OCO}$ were considered the free parameters. The potential energy diagram for the reaction proceeding via CO_2^{2+} (5A_1) to the final products $\text{C}^+({}^2P) + \text{O}_2^+({}^2\Pi_g)$ is shown in Figure 4.

After the collision with the projectile, (A) the neutral CO_2 molecule becomes a dication within the Franck–Condon region, further, the molecular ion dynamically approaches (B) the minimum of the potential energy surface at $R = 1.29$ Å, $\angle\text{OCO} = 115^\circ$, and passing through the (C) transition state at $R = 2.48$ Å, $\angle\text{OCO} = 65^\circ$ to finally dissociate to (D) the products $\text{C}^+({}^2P)$ and $\text{O}_2^+({}^2\Pi_g)$.

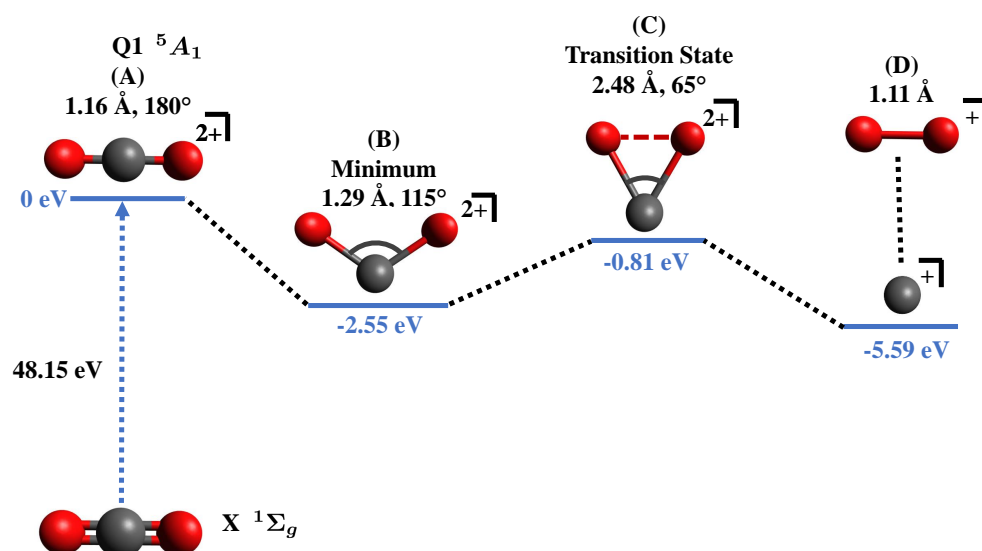


Figure 4. Relevant points in the potential energy surface of CO_2^{2+} in the 5A_1 state showing possible pathway for O_2^+ formation. Shown are (A) Excitation to the dicationic state in the Franck–Condon region, (B) equilibrium configuration of the 5A_1 state, (C) existence of a transition state between reactants and products, and (D) final products. Shown are the bond lengths and bond angles corresponding to each geometry. Q1 represents the first excited state in the quintet manifold. The “0 eV” in blue color acts as a reference for other points along the surface.

To check for any angular dependence of the fragments, we show in Figure 5 the angular distribution of the C^+ and O_2^+ daughter ions. The result is consistent with that reported by Zhao et al. [13] that the fragments are distributed isotropically with respect to the projectile beam axis. The reason for this, as mentioned by Zhao et al. is that the lifetime of the CO_2^{2+} ion is larger than its rotational period; during bending and bond rearrangement, the molecular ion is rotating, thus losing any angular information.

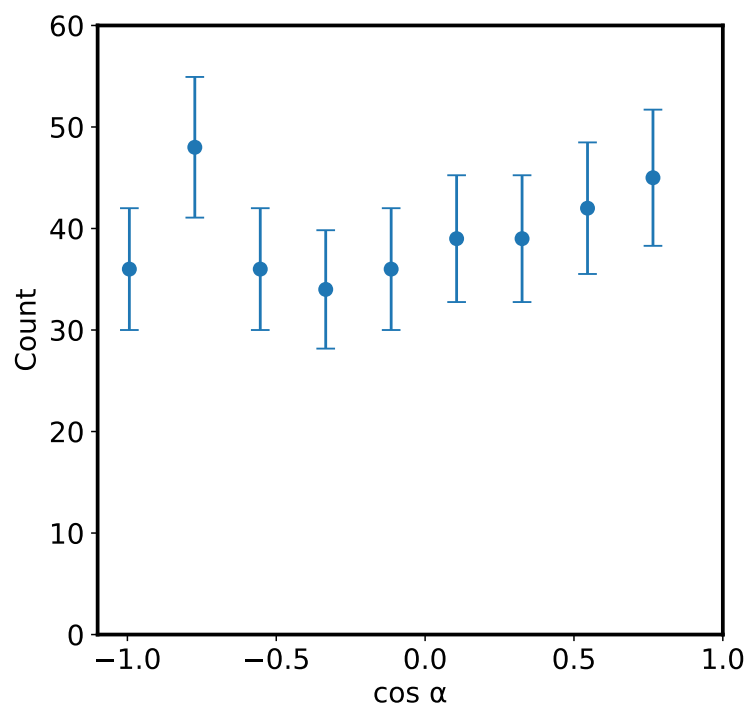


Figure 5. Plot showing isotropic fragmentation pattern of the C^+ ions upon 200 keV Xe^{10+} impact. α is the detection angle of C^+ ions with respect to the projectile beam direction.

4. Branching Ratio

As is vital from an environmental perspective, the transformation of pollutant CO_2 into O_2 makes it possible to study this channel in a deeper sense. One of the fundamental questions to address is about the strength of this channel. In their study on the bond rearrangement of CO_2 molecules, Zhao et al. [13] reported a branching ratio of $0.0796 \pm 0.0058\%$, among all the fragmentation channels of the dication following strong field ionization of the neutral CO_2 molecules. In another study, Yuan et al. [19] reported a 1.7% branching ratio of the $C^+ + O_2^+$ channel fragmenting into $C^+ + O^+ + O$. Other than these two studies, to the best of our knowledge, the branching ratio for this channel is not mentioned anywhere else. In this subsection, we report the branching ratio of this channel with respect to the sum of bond rearrangement and the most probable channel $O^+ + CO^+$, which is shown in Table 1. From this table, we observe that for all ion impacts, the branching ratio of this channel with respect to $O^+ + CO^+$ remains almost the same. In the current velocity regime of the projectile ions (≤ 1 a.u.), electron capture is the most dominant mechanism of preparing the dication. It is well known that during electron capture, the projectile ion mostly interacts with the valence electrons of the target, thus leading to populations in ground or lower excited states. Such collisions are also termed soft collisions. The independence of the strength of the bond rearrangement channel on projectile charge and velocity reflects that in the present velocity regime, soft collisions during electron capture populate the molecular dication in the 5A_1 electronic state with almost equal strength, responsible for the bond rearrangement channel. It requires more such experiments to study the cross-section of the bond-rearrangement channel in velocity higher than 1 a.u.

Table 1. Branching ratio between $C^+ + O_2^+$ and $O^+ + CO^+$ channels across different projectile ion impacts, to the second decimal point, estimated with the present experimental data. Counts in both the channels are added and the branching ratio with respect to the sum is tabulated. The uncertainties are statistical uncertainties. Perturbation strength (q/v_p) is also listed, rounded to the nearest integer.

S. No.	Beam	q/v_p	Branching Ratio
			$C^+ + O_2^+ : O^+ + CO^+$
1	240 keV Ar ³⁺	6	0.15 ± 0.01 : 99.85 ± 0.01
2	62 keV Ar ³⁺	12	0.17 ± 0.01 : 99.83 ± 0.01
3	240 keV Ar ⁶⁺	12	0.17 ± 0.01 : 99.83 ± 0.01
4	240 keV Ar ⁸⁺	16	0.18 ± 0.01 : 99.83 ± 0.01
5	160 keV Ar ⁸⁺	20	0.17 ± 0.02 : 99.83 ± 0.02
6	200 keV Xe ¹⁰⁺	40	0.15 ± 0.01 : 99.85 ± 0.01

5. Conclusions

We observed the signatures of molecular oxygen formation as a consequence of bond rearrangement, due to electron-capture-induced fragmentation of CO₂ molecules. We proposed that symmetric stretching of the two C–O bonds and bending are the responsible mechanisms of the bond rearrangement. With ab initio quantum chemistry calculations, we found out that ⁵A₁ is the electronic state responsible for KER around 5.74 ± 0.2 eV. We found a transition state in the potential energy surface of this state with no energy barrier to the reaction. We hope that the electronic state found here will be of use to enhance the cross-section of this channel using state-selective ionization methods.

The branching ratios of the bond-rearrangement channel are found to be independent of the perturbation strength, reflecting that in the present velocity regime, the ⁵A₁ electronic state is populated with similar strength during the collision. More experiments are required to explore this channel in the high-velocity regime.

Author Contributions: Conceptualization, K.K. and D.M.; Methodology, D.M. and K.K.; Validation, D.M.; Formal analysis, K.K. and D.M.; Investigation, K.K. and D.M.; Resources, D.M.; Data curation, K.K., J.M. and H.S.; Writing—original draft preparation, K.K.; Writing—review and editing, D.M.; Visualization, K.K.; Supervision, D.M.; Project administration, D.M.; Funding acquisition, D.M. All authors have read and agreed to the published version of the manuscript.

Funding: This work is supported by the Department of Atomic Energy (Government of India) under Research Project No. RTI 4002.

Data Availability Statement: Data will be available upon reasonable request.

Acknowledgments: We thank Vaibhav Prabhudesai for the fruitful discussions regarding the dynamics involved, Vamsee K. Voora in understanding the concepts related to the theoretical calculations, and A.K.A. Siddiki for helping in the experiments and fruitful discussions. We also thank the entire technical staff of the TIFR-ECRIA facility for smooth operation during the experiment.

Conflicts of Interest: The authors declare no conflicts of interest.

References

1. Hecht, M.H.; Hoffman, J.; Team, M. The Mars oxygen ISRU experiment (MOXIE) on the Mars 2020 Rover. In Proceedings of the 3rd International Workshop on Instrumentation for Planetary Mission, Pasadena, CA, USA, 24–27 October 2016; Volume 1980, p. 4130.
2. Hu, H.; Larimian, S.; Erattupuzha, S.; Wen, J.; Baltuška, A.; Kitzler-Zeiler, M.; Xie, X. Laser-induced dissociative recombination of carbon dioxide. *Phys. Rev. Res.* **2019**, *1*, 033152. [[CrossRef](#)]
3. Zhang, S.; Wang, X.; Jiang, W.; Zhang, Y.; Jiang, Y.; Zhu, Z. Charge-encoded multi-photoion coincidence for three-body fragmentation of CO₂ in the strong laser fields. *J. Chem. Phys.* **2022**, *156*, 134302. [[CrossRef](#)] [[PubMed](#)]
4. Srivastav, S.; Bapat, B. Electron-impact-like feature in triple fragmentation of CO₂³⁺ under slow proton impact. *Phys. Rev. A* **2022**, *105*, 012801. [[CrossRef](#)]
5. Duley, A.; Kelkar, A.H. Fragmentation Dynamics of CO₂ q + (q = 2,3) in Collisions with 1 MeV Proton. *Atoms* **2023**, *11*, 75. [[CrossRef](#)]

6. Chueh, W.C.; Falter, C.; Abbott, M.; Scipio, D.; Furler, P.; Haile, S.M.; Steinfeld, A. High-Flux Solar-Driven Thermochemical Dissociation of CO₂ and H₂O Using Nonstoichiometric Ceria. *Science* **2010**, *330*, 1797–1801. [[CrossRef](#)] [[PubMed](#)]
7. Hwang, D.Y.; Mebel, A.M. Ab initio study of spin-forbidden unimolecular decomposition of carbon dioxide. *Chem. Phys.* **2000**, *256*, 169–176. [[CrossRef](#)]
8. Grebenshchikov, S.Y. Photodissociation of carbon dioxide in singlet valence electronic states. I. Six multiply intersecting ab initio potential energy surfaces. *J. Chem. Phys.* **2013**, *138*, 224106. [[CrossRef](#)]
9. Lu, Z.; Chang, Y.C.; Yin, Q.Z.; Ng, C.Y.; Jackson, W.M. Evidence for direct molecular oxygen production in CO₂ photodissociation. *Science* **2014**, *346*, 61–64. [[CrossRef](#)] [[PubMed](#)]
10. Wang, X.D.; Gao, X.F.; Xuan, C.J.; Tian, S.X. Dissociative electron attachment to CO₂ produces molecular oxygen. *Nat. Chem.* **2016**, *8*, 258–263. [[CrossRef](#)] [[PubMed](#)]
11. Larimian, S.; Erattupuzha, S.; Mai, S.; Marquetand, P.; González, L.; Baltuška, A.; Kitzler, M.; Xie, X. Molecular oxygen observed by direct photoproduction from carbon dioxide. *Phys. Rev. A* **2017**, *95*, 011404. [[CrossRef](#)]
12. Long, J.; Furch, F.J.; Durá, J.; Tremsin, A.S.; Vallerga, J.; Schulz, C.P.; Rouzée, A.; Vrakking, M.J.J. Ion-ion coincidence imaging at high event rate using an in-vacuum pixel detector. *J. Chem. Phys.* **2017**, *147*, 013919. [[CrossRef](#)] [[PubMed](#)]
13. Zhao, S.; Jochim, B.; Feizollah, P.; Rajput, J.; Ziaee, F.; P., K.R.; Kaderiya, B.; Borne, K.; Malakar, Y.; Berry, B.; et al. Strong-field-induced bond rearrangement in triatomic molecules. *Phys. Rev. A* **2019**, *99*, 053412. [[CrossRef](#)]
14. Öhrwall, G.; Sant’Anna, M.M.; Stolte, W.C.; Dominguez-Lopez, I.; Dang, L.T.N.; Schlachter, A.S.; Lindle, D.W. Anion and cation formation following core-level photoexcitation of CO₂. *J. Phys. B At. Mol. Opt. Phys.* **2002**, *35*, 4543. [[CrossRef](#)]
15. Laksman, J.; Månsson, E.P.; Grunewald, C.; Sankari, A.; Gisselbrecht, M.; Céolin, D.; Sorensen, S.L. Role of the Renner-Teller effect after core hole excitation in the dissociation dynamics of carbon dioxide dication. *J. Chem. Phys.* **2012**, *136*, 104303. [[CrossRef](#)] [[PubMed](#)]
16. Eland, J.H.D.; Zagorodskikh, S.; Squibb, R.J.; Mucke, M.; Sorensen, S.L.; Feifel, R. Carbon dioxide ion dissociations after inner shell excitation and ionization: The origin of site-specific effects. *J. Chem. Phys.* **2014**, *140*, 184305. [[CrossRef](#)] [[PubMed](#)]
17. Yao, Y.; Shushkov, P.; Miller III, T.F.; Giapis, K.P. Direct dioxygen evolution in collisions of carbon dioxide with surfaces. *Nat. Commun.* **2019**, *10*, 2294. [[CrossRef](#)]
18. Smita, G.; Barreiro-Lage, D.; Walsh, N.; Bart, O.; Sorensen, S.L.; Díaz-Tendero, S.; Mathieu, G. The origin of enhanced O² production from photoionized CO₂ clusters. *Commun. Chem.* **2022**, *5*, 16. [[CrossRef](#)]
19. Yuan, H.; Xu, S.; Wang, E.; Xu, J.; Gao, Y.; Zhu, X.; Guo, D.; Ma, B.; Zhao, D.; Zhang, S.; et al. Fragmentation Dynamics of a Carbon Dioxide Dication Produced by Ion Impact. *J. Phys. Chem. Lett.* **2022**, *13*, 7594–7599. [[CrossRef](#)] [[PubMed](#)]
20. Dörner, R.; Mergel, V.; Jagutzki, O.; Spielberger, L.; Ullrich, J.; Moshhammer, R.; Schmidt-Böcking, H. Cold Target Recoil Ion Momentum Spectroscopy: A ‘momentum microscope’ to view atomic collision dynamics. *Phys. Rep.* **2000**, *330*, 95–192. [[CrossRef](#)]
21. Ullrich, J.; Moshhammer, R.; Dorn, A.; Dörner, R.; Schmidt, L.P.H.; Schmidt-Böcking, H. Recoil-ion and electron momentum spectroscopy: Reaction-microscopes. *Rep. Prog. Phys.* **2003**, *66*, 1463. [[CrossRef](#)]
22. Agnihotri, A.N.; Kelkar, A.H.; Kasthurirangan, S.; Thulasiram, K.V.; Desai, C.A.; Fernandez, W.A.; Tribedi, L.C. An ECR ion source-based low-energy ion accelerator: Development and performance. *Phys. Scr.* **2011**, *2011*, 014038. [[CrossRef](#)]
23. Khan, A.; Tribedi, L.C.; Misra, D. A recoil ion momentum spectrometer for molecular and atomic fragmentation studies. *Rev. Sci. Instrum.* **2015**, *86*, 043105. [[CrossRef](#)] [[PubMed](#)]
24. Siddiki, M.A.K.A.; Nrisimhamurthy, M.; Kumar, K.; Mukherjee, J.; Tribedi, L.C.; Khan, A.; Misra, D. Development of a cold target recoil ion momentum spectrometer and a projectile charge state analyzer setup to study electron transfer processes in highly charged ion–atom/molecule collisions. *Rev. Sci. Instrum.* **2022**, *93*, 113313. [[CrossRef](#)] [[PubMed](#)]
25. Matthews, D.A.; Cheng, L.; Harding, M.E.; Lipparini, F.; Stopkowicz, S.; Jagau, T.C.; Szalay, P.G.; Gauss, J.; Stanton, J.F. Coupled-cluster techniques for computational chemistry: The CFOUR program package. *J. Chem. Phys.* **2020**, *152*, 214108. [[CrossRef](#)] [[PubMed](#)]
26. Stanton, J.F.; Bartlett, R.J. The equation of motion coupled-cluster method. A systematic biorthogonal approach to molecular excitation energies, transition probabilities, and excited state properties. *J. Chem. Phys.* **1993**, *98*, 7029–7039. [[CrossRef](#)]
27. Goings, J.J.; Caricato, M.; Frisch, M.J.; Li, X. Assessment of low-scaling approximations to the equation of motion coupled-cluster singles and doubles equations. *J. Chem. Phys.* **2014**, *141*, 164116. [[CrossRef](#)] [[PubMed](#)]
28. Koch, H.; Jørgensen, P. Coupled cluster response functions. *J. Chem. Phys.* **1990**, *93*, 3333–3344. [[CrossRef](#)]
29. Caricato, M. Exploring Potential Energy Surfaces of Electronic Excited States in Solution with the EOM-CCSD-PCM Method. *J. Chem. Theory Comput.* **2012**, *8*, 5081–5091. [[CrossRef](#)] [[PubMed](#)]
30. Dunning, T.H., Jr. Gaussian basis sets for use in correlated molecular calculations. I. The atoms boron through neon and hydrogen. *J. Chem. Phys.* **1989**, *90*, 1007–1023. [[CrossRef](#)]
31. Møller, C.; Plesset, M.S. Note on an Approximation Treatment for Many-Electron Systems. *Phys. Rev.* **1934**, *46*, 618–622. [[CrossRef](#)]
32. Pople, J.A.; Nesbet, R.K. Self-Consistent Orbitals for Radicals. *J. Chem. Phys.* **1954**, *22*, 571–572. [[CrossRef](#)]

Disclaimer/Publisher’s Note: The statements, opinions and data contained in all publications are solely those of the individual author(s) and contributor(s) and not of MDPI and/or the editor(s). MDPI and/or the editor(s) disclaim responsibility for any injury to people or property resulting from any ideas, methods, instructions or products referred to in the content.